Journal of Renewable Energies

Revue des Energies Renouvelables

journal home page: https://revue.cder.dz/index.php/rer

Research paper

Use of the dual stator induction machine in a hybrid renewable energy pumping system

Arezki Adjati [a,*], **Toufik Rekioua** [a], **Djamila Rekioua** [a,]

[a] *Industrial and Information Technology Laboratory, Faculty of Technology, A.Mira University, Bejaia, Algeria*

ARTICLE INFO

Article history:
Received April 1, 2024
Accepted April 22, 2024

Keywords:
Dual stator induction motor
Photovoltaic generator
Centrifugal pump
Wind turbine
Fuel cell

ABSTRACT

In this article, we propose a hybrid power supply of a water pumping station. The combination of photovoltaic, wind turbine, and fuel cell powers the dual stator inductor motor that drives the centrifugal pump. The novelty of this contribution is to replace the usual actuators used for pumping by a dual stator inductor motor that offers power segmentation and the possibility to operate in degraded mode. The adoption of Fuel Cells helps get rid of carbon dioxide to migrate to hydrogen.

1. INTRODUCTION

Bernal-Agustin & al (Bernal &al, 2009) insist on the need for the adoption of hybridization in remote, off-grid areas. Bajpai and Dash (Bajpai, Dash, 2012) offer hybridization to any stand-alone application to provide uninterrupted power without greenhouse gas emissions. Zarour (Zarour, 2010) ensured through his study, the complementarity between solar and wind energy. Bouzidi (Bouzidi, 2011) through his efforts, has summarized through a comparative study, the advantages and disadvantages of photovoltaic and wind systems. Hajdidj et al (Hadjidj & al,2017) introduced a battery storage system in the PV-wind hybrid system and stated that the failure of one of the sources is the main obstacle to energy production for hybrid systems. Ipsakis and his team (Ipkasis & al, 2009) proposed management strategies for a hybrid system with hydrogen storage. Dufo-Lapez (Dufo & al, 2009) drew the intention on the additional cost of hydrogen storage compared to conventional systems.

In this contribution, it is wise to study the behavior of the sources involved to ensure continuity of service despite the random characteristics of renewable energies. The adoption of the DSIM must ensure the continuity of pumping even if half of the power phases are out of service.

* *Corresponding author, E-mail address: arezki.adjati@univ-bejaia.dz*
Tel : + 213 771915663

ISSN: 1112-2242 / EISSN: 2716-8247

2. COMPONENTS OF HYBRID PUMPING SYSTEM

To ensure the continuous supply of water to a locality we proposed a combination illustrated in Figure 1. The system contains a photovoltaic power generator (GPV), a wind turbine that drives a double-star asynchronous generator (DSIG), and a fuel cell (FC) as energy sources used to power a double-star asynchronous motor (DSIM) used to drive a centrifugal pump and power an electrolyzer to produce hydrogen.

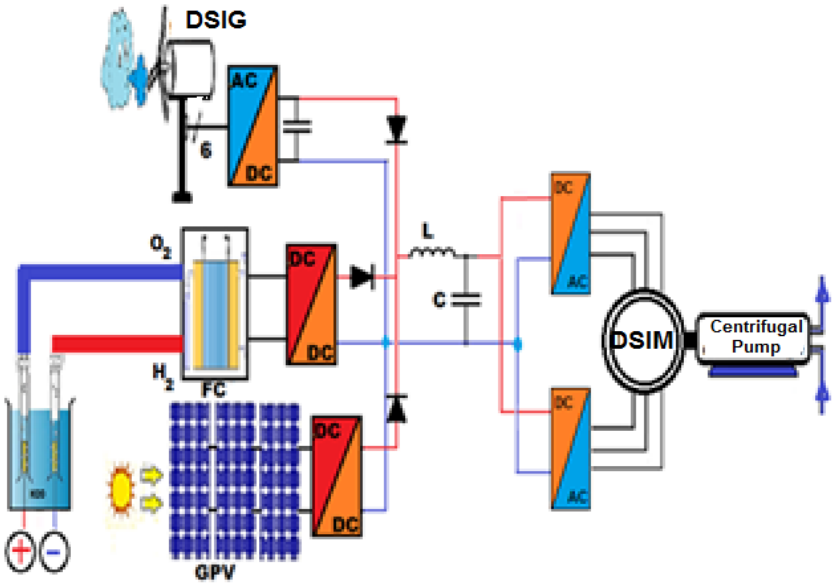

Fig 1. Hybrid photovoltaic-wind-FC installation (Adjati, 2022)

3. MODELLING OF THE PHOTOVOLTAIC GENERATOR

To improve the efficiency of the GPV, mathematical models were developed to identify the multiple parameters having non-linear behavior to be able to control them (Adjati 2014).

$$\left|\begin{array}{l} V_G = n_s.V \\ I_G = n_p.I \\ I_{rp} = n_p.i_{rp} \\ R_p = \dfrac{n_s}{n_p}.r_p \end{array}\right. \quad and \quad \left|\begin{array}{l} V_d = n_s.v_d \\ I_d = n_p.i_d \\ I_{ph} = n_p.i_{ph} \\ R_s = \dfrac{n_s}{n_p}.r_s \end{array}\right. \qquad (1)$$

In the case where all the cells used are identical and operate under the same conditions, figure (2) represents the equivalent electrical diagram of the GPV (Adjati; 2022).

Each group of panels requires an «np» number of branches in parallel consisting of several cells «ns» in series.

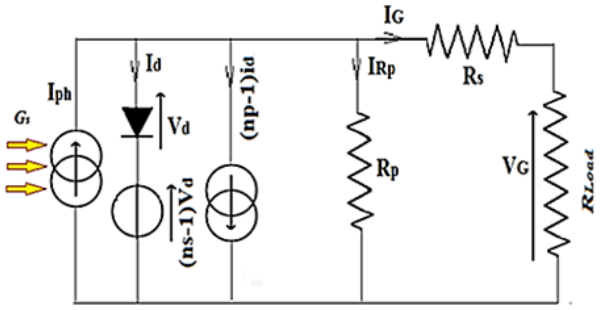

Fig 2. Electrical diagram of a group of panels "single diode model" (Adjati, 2022).

The following relation gives the current delivered by the photovoltaic panel (Adjati, 2022):

$$I_G = P_1 G_s + P_1 P_2 G_s\left(G_s - G_{sref}\right) + P_1 P_3 G_s\left(T_j - T_{jref}\right) - \frac{V_G + R_s I_G}{R_p} . -P_4 T_j^3 exp\left(\frac{-E_g}{K.T_j}\right)\left[exp\left(\frac{e(V_G + R_s I_G)}{A.K.T_j}\right) - 1\right] \quad (2)$$

The coefficients A, P1, P2, P3, and P4 are: $P_1 = 0.00345$; $P_2 = \frac{P_4}{V_{co}}$; $P_3 = ln\left(\frac{I_{cc}(1+P_1)-I_m}{P_1 I_{cc}}\right)$ $P_4 = ln\left(\frac{1+P_1}{P_1}\right)$; $A = ln\left(\frac{P_3}{P_4}\right)/ln\left(\frac{V_m}{V_{co}}\right)$

4. WIND TURBINE MODELING

The wind turns the turbine, which picks up some of the energy swept by the blades and transfers it to the hub attached to the turbine shaft, which then transmits the mechanical energy to the DSIG via a speed multiplier.

4.1 Theoretically recoverable available wind energy

The kinetic energy as a function of mass and wind speed is (Adjati, 2021):

$$E_c = \frac{1}{2} m v^2 \quad (3)$$

The average available power contained in the form of kinetic energy associated with a displacement of an available air mass on a surface S [m²] of a wind turbine is [8, 12]:

$$P = \frac{1}{2} \rho_{air} S v^3 \quad (4)$$

4.2 Really recoverable wind energy

Wind energy truly recoverable is;

$$P_{recup} = \frac{1}{2} . \frac{16}{27} \rho S v_1^3 = \frac{1}{2} C_p \rho S v_1^3 \quad (5)$$

4.3 Power coefficient Cp

For a small wind turbine, the analytical equation of the power coefficient Cp as a function of λ is (Kasbadji & al,2003):

$$C_p(\lambda) = 7{,}9563.10^{-5}\lambda^5 - 17{,}375.10^{-4}\lambda^4 - 9{,}86.10^{-3}\lambda^3 - 9{,}41.10^{-3}\lambda^2 + 6{,}38.10^{-2}\lambda + 0.001 \quad (6)$$

4.4 Aerodynamic power

With R[m] the length of a blade, the aerodynamic power is [8, 14]:

$$P_{wind} = \frac{1}{2}\rho\pi R^2 C_p(\lambda) v^3 \quad (7)$$

4.5 Turbine torque

The turbine toque is [8, 14]:

$$C_T = \frac{P_T}{\Omega_T} = \frac{1}{2}\rho\pi R^3 C_p(\lambda) v^2 \quad (8)$$

5. DUAL STATOR INDUCTION GENERATOR STUDY

The capacitors used for self-priming of the GASDE, represented by Figure 3 have a value of 40µF. The rectifier is a double parallel PD3. Two rectifiers were used for the two stars of the DSIG (Adjati 2022).

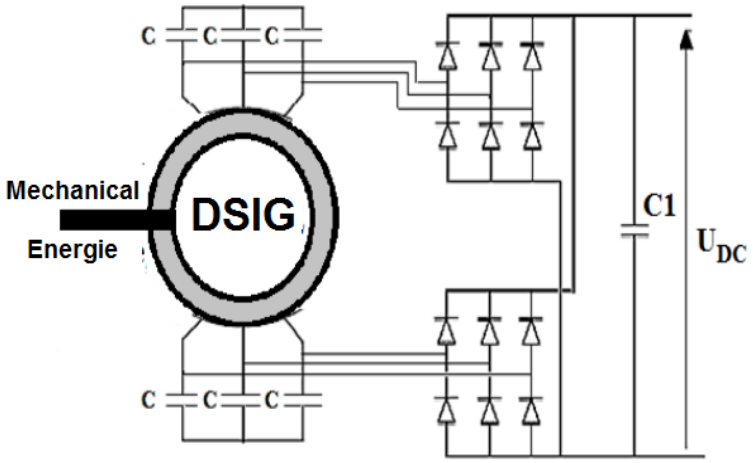

Fig 3. Dual PD3 rectifier of the voltage generated by the DSIG (Adjati, 2022)

The average value of the rectified voltage is (Adjati, 2022):

$$U_{dc} = \sqrt{3}\, V_m \frac{sin\frac{\pi}{6}}{\frac{\pi}{6}} \quad (9)$$

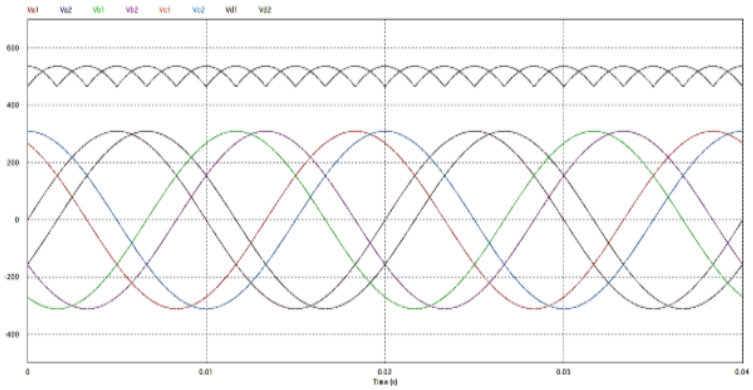

Fig 4. Voltage at Rectifier Inlet and Outlet (PSIM)

In addition, the effective value of the straightened tension is:

$$U_{eff} = V_m \times \sqrt{\frac{3\times\left(1+sin\frac{2\pi}{6}\right)}{2\times\frac{2\pi}{6}}} \tag{10}$$

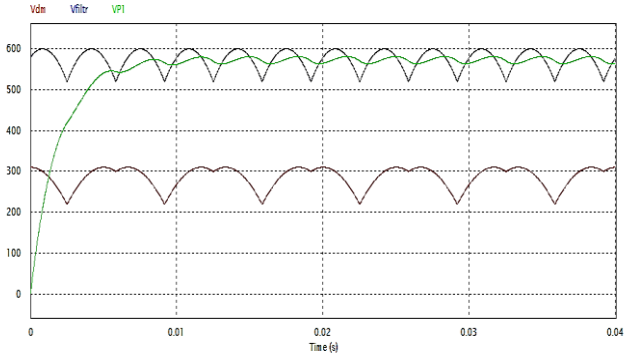

Fig 5. Shape of rectified voltages (PSIM)

Figures 4 and 5 show that the output voltage of the rectifier is composed of the sum of the two rectified voltages with a frequency equal to 6 times the frequency of the source.

To be able to power the DSIM inverters, the voltages generated by the GSID are converted.

6. FUEL CELL MODELING

PEMFC technology allows a low operating temperature not exceeding 100°C and has a rapid start-up and easy heat dissipation (Adjati; 2020).

The hydrogen cell uses hydrogen as a fuel, and oxygen as an oxidizer, usually taken from ambient air. The hydrogen used is either stored in compressed gas cylinders or metal hydrides or produced by water reforming of different fuels (Cropper & al, 2004).

To describe the chemical reactions at the anode and cathode levels of the FC, several models exist in the literature, including that of the evolution of the voltage, which combines empirical models with elementary laws (Adjati 2022).

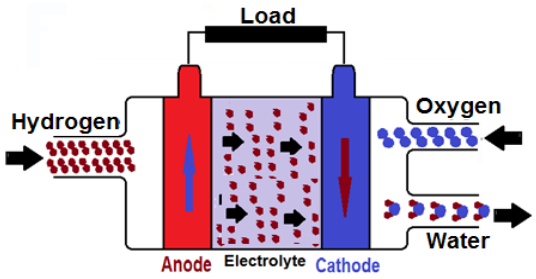

Fig 6. Proton exchange membrane Fuel Cell "PEMFC" (Cropper, 2004).

Indeed, Maxwell's equations model the transport of matter, Nernst's equations, the thermodynamic equilibrium potentials, and Tafel's equations take care of activation overvoltage. Nernst-Planck equations determine internal resistance (Adjati, 2020).

This equation gives the global real potential of the Proton Exchange Membrane Fuel Cells (PEMFC):

$$U_{FC} = E_{Nernst} - V_{act} - V_{ohm} - V_{conc} \tag{11}$$

The equivalent electrical circuit represents the dynamic behavior of the fuel cell :

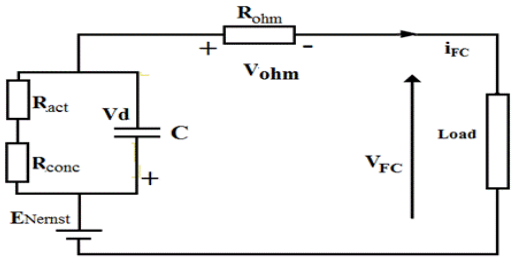

Fig 7. Equivalent dynamic electrical diagram of an FC (Adjati; 2020).

TAFEL equation gives the activation losses:

$$V_{act} = A \times \ln\left(\frac{I_{FC}+I_n}{i_0}\right) \tag{12}$$

The ohmic losses with Rm total resistance of the FC:

$$V_{ohm} = R_m \times (I_{FC} + I_n) \tag{13}$$

The Concentration losses:

$$V_{conc} = -B \times \ln\left(1 - \frac{I_{FC}+I_n}{I_L}\right) \tag{14}$$

Nernst voltage is the thermodynamic equilibrium potential defined for standard temperature and pressure values and is written as follows (Adjati; 2020):

$$E_{nernst} = 1.229 - 0.85.10^{-3}(T - 298.15) + 4.31.10^{-5}T\left[\ln(PH_2) + \frac{1}{2}\ln(PO_2)\right] \tag{15}$$

The temperature of the membrane and the partial pressures of the gas vary proportionally as a function of the current, on the other hand, the pressures of hydrogen and oxygen vary inversely with variations in the current (Adjati; 2020).

7. PUMP MODELLING

The pumping rate "Q" is the amount of water that a pump can move during a given time interval. The static level is the distance from the ground to the surface of the water before pumping and is named the dynamic level for pumping at an average flow. The difference between these two levels is called drawdown.

7.1 Total dynamic head (TDH)

To convey a liquid, the pump should provide some pressure called TDH. This is the pressure difference in meters of water gauge (mwg) between the aspiration and discharge orifices (Adjati, 2022).

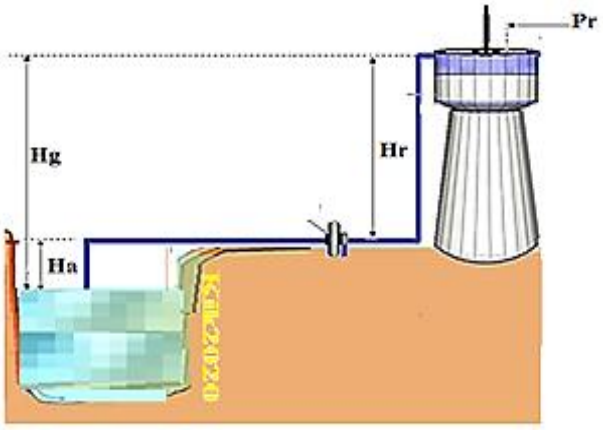

Fig 8. Surface Pump (Adjati, 2022).

The expression of TDH is (Adjati, 2022):

$$\mathrm{TDH} = \mathrm{H_g} + (\mathrm{J}_a + \mathrm{J_r}) + \mathrm{P_r} \tag{16}$$

The TDH is the sum of the residual pressure at the outlet of the delivery tube and the geometric height also known as the total delivery height and the pressure losses "Jc" in the suction tube, the strainer, the valve, the or valves, etc.

The geometric height "Hg" is only the sum of the suction height "Ha" and that of the discharge "Hr". "Jc" represents the overall pressure losses at suction and discharge.

$$\mathrm{TDH} = (\mathrm{H_a} + \mathrm{H_r}) + \mathrm{J}_c + \mathrm{P_r} \tag{17}$$

There are standardized values of pressure losses expressed as a percentage of the geometric height depending on the flow rate and the section of the pipes provided by the manufacturer in the form of tables.

Practically, to calculate pressure losses 10% to 15% of the geometric height are used (Adjati, 2022).

7.2 Pump power

According to Bernoulli's theorem, the hydraulic power supplied by the pump is:

$$\mathrm{P_h} = \rho_{water} \times \mathrm{g}_t \times \mathrm{Q} \times \mathrm{HMT} \tag{18}$$

BRAUNSTEIN and KORNFELD introduced in 1981 the expression of mechanical power (Adjati, 2022).

$$P_{mec} = \mathrm{K}_r \times \omega_r^3 \tag{19}$$

The centrifugal pump opposes a resistant torque from which its expression is:

$$T_r = \mathrm{K}_r \times \omega_r^2 + T_s \tag{20}$$

PELEIDER PETERMAN gives the model identified by the expression of the TDH (Adjati, 2012):

$$\mathrm{TDH} = \mathrm{K}_0 \times \omega_r^2 + K_1 \omega_r Q - K_2 Q^2 \tag{21}$$

8. DUAL STATOR INDUCTION MACHINE MODELING

8.1 Magnetic power

The expression of magnetic energy is:

$$\mathrm{w_{mag}} = \left[[\mathrm{i_{s1}}]^{\mathrm{t}}[\varphi_{\mathrm{s1}}] + [\mathrm{i_{s2}}]^{\mathrm{t}}[\varphi_{\mathrm{s2}}] + [\mathrm{i_r}]^{\mathrm{t}}[\varphi_{\mathrm{r}}]\right]/2 \tag{22}$$

8.2 Electromagnetic torque

The partial derivative of the energy concerning the mechanical angle θm gives the electromagnetic torque (Adjati, 2022).

$$\mathrm{C_{em}} = \frac{\mathrm{dw_{mag}}}{\mathrm{d\theta_m}} = \mathrm{p} \times \frac{\mathrm{dw_{mag}}}{\mathrm{d\theta_e}} \tag{23}$$

p represents the number of pole pairs and θe= θr the electrical angle, the torque expression becomes (Adjati, 2022):

8.3 Mechanical equation

The movement of the rotor is:

$$\mathrm{J} \times \frac{\mathrm{d\Omega}}{\mathrm{dt}} = \mathrm{C_{em}} - \mathrm{C}_r - \mathrm{f}_r \times \Omega \tag{24}$$

8.4 Inverter modeling

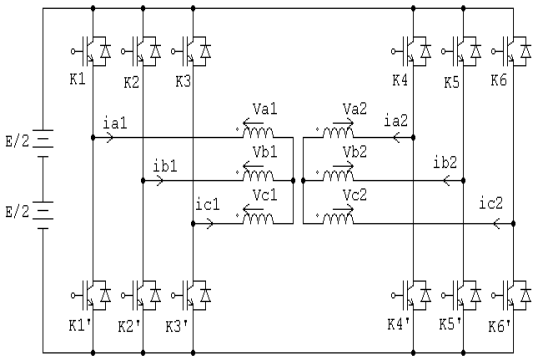

Fig 9. The power supply of the stator by voltage inverters (Adjati, 2022).

Two three-phase inverters, with controlled switches used to power the two stars of the machine.

Control by sine-triangle pulse width modulation 'PWM' consists of comparing a low-frequency modulating wave called 'reference voltage' to a high-frequency triangular-shaped carrier wave (Hamitouche & al, 2020).

9. Pumping station sizing

The actual water needs of this locality during the year must be determined, to predict the capacity of the reservoir and the pumping time (Adjati, 2022).

Table 1. Pumping data

Pumping time	9 hours	Inverter efficiency	0.95
Tank volume	150 m3	DSIM efficiency	0.85
Flow	17m3/h	Pump efficiency	0.55
Total dynamic head	30 m	Total efficiency	0.444

Under an expected nominal flow rate of Qn=17 m3/h and a total dynamic head TDH=30, the pumping time is approximately 9 hours. Table 1 groups the results found after a rigorous design basis (Adjati, 2022).

Table 2. Dimensions of the renewable sources (Adjati, 2022).

Photovoltaic generator		**Wind turbine**		**Fuel Cell**	
Normalized power	3960W	Mechanic power	5000W	Number of cells	1000
Number of serial panels	18	Blade radius	5 m	Electric current	6.29 A
Number of parallel panels	2	DSIG efficiency	0.88	Surface	4.83 cm²
		Multiplier gain	0.90	Fuel	Hydrogen
Number of panels	36	Multiplier	30.5	Oxidizer	Oxygen

10. RESULTS AND COMMENTS

The points of intersection between the carrier and the modulator determine the switching times. The carrier sets the switching frequency of the switches.

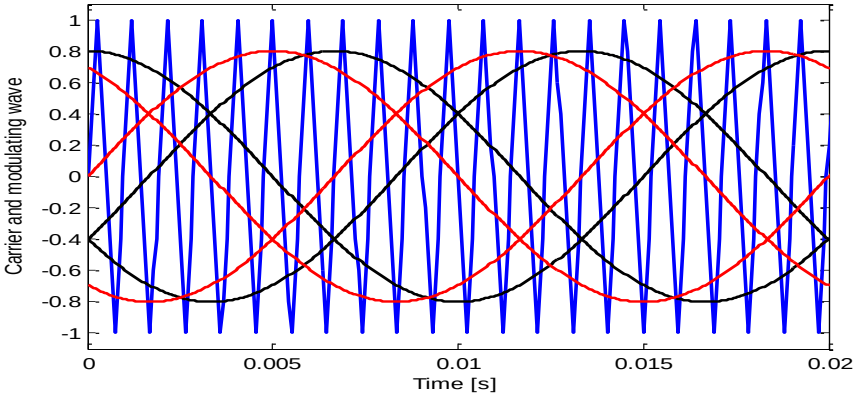

Fig 10. PWM working principle

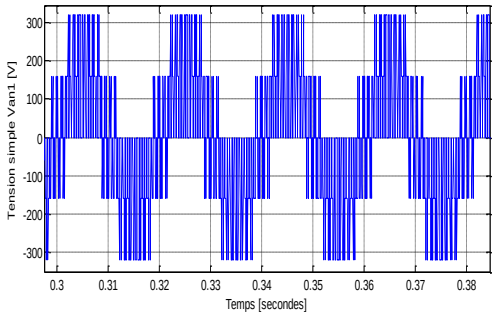

Fig 11. Voltage from the inverter Va1

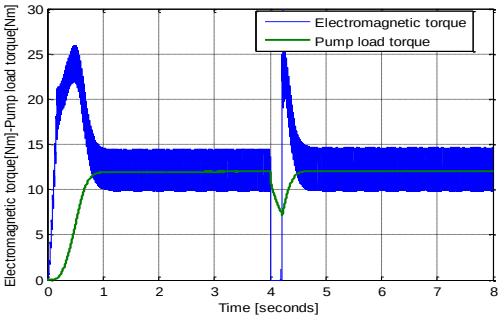

Fig 12. Electromagnetic & Resistive torque

At start-up, the torque of the machine oscillates, reaching 26 Nm (Fig. 12), before stabilizing, with some ripples, around a value of 12.5 Nm. The pump, in turn, opposes a resistant torque, which increases rapidly, for a period of 0.8 s, before following the evolution of the engine torque. Figure 13 confirms the quadratic relationship between TDH and rotation speed. Figure 14 shows the evolution of the water flow and the TDH. To have a flow in the pipes, it would be necessary that the pump reach a certain speed of rotation obtained after a few moments.

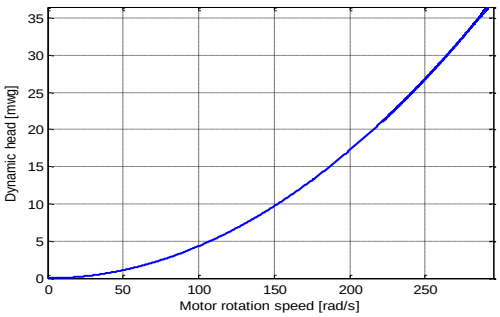

Fig 13. Dynamic head vs Motor rotation speed

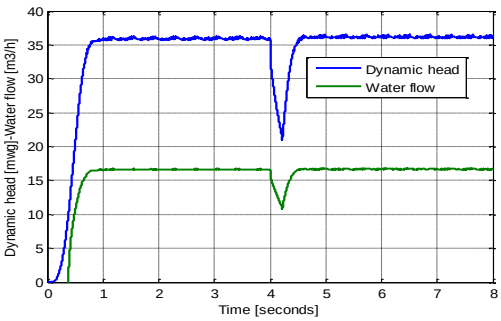

Fig 14. TDH and water flow versus time

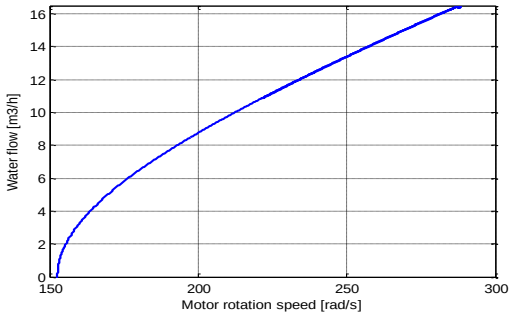

Fig 15. Water Flow vs Motor rotation speed

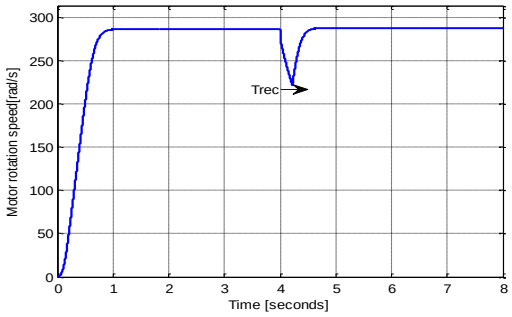

Fig 16. Motor rotation speed

From Figure 15, the pump will start pumping water if and only if the rotation speed is beyond the threshold speed, which is equal to 151 rad/sec. It is also interesting to note that the speed of rotation of the engine and the water flow are directly proportional.

The pump torque, rotation speed, pumped flow, and HMT depend on the variation of the sunshine. However, the use of the maximum power search technique can overcome the handicap of low lighting.

In the case of the absence of the sun and a solicitation of pumping after a decrease in the level of the tank, the fuel cell will ensure the relay. The FC offers a continuous voltage to the two inverters used to power the asynchronous motor with dual star, thus training the pump.

11. CONCLUSION

We proposed a hybrid power supply composed of a photovoltaic generator, a wind turbine, and a fuel cell using hydrogen obtained by an electrolyzer to power the pumping station isolated from the conventional power grid.

With this hybridization, renewable sources are complementary instead of being competitive, a way to counteract the intermittent natures of these sources.

We chose the DSIM to run a centrifugal pump and the DSIG as the wind turbine generator. This choice is justified by the segmentation of power and the increase of the service life of the installation or by the possibility of operation in degraded mode, offering an additional degree of freedom.

The flow rates pumped during a day are increased compared to single source systems and the operating strategy directly influences the performance, efficiency, and service life of the installation.

REFERENCES

Adjati A. (2012) Etude des machines asynchrones à double étoile en pompage, Thèse de Magister de l'université A. Mira Bejaia, systèmes électro-énergétique.

Adjati A., Azib A., Rekioua T. (2014) Etude d'une machine asynchrone à double alimentation en pompage photovoltaïque, Revue des Energies Renouvelables, Vol. 17 N°3 411 – 418.

Adjati A., Rekioua T., Rekioua, D. (2020) Study of dual stator induction motor in photovoltaic-fuel cell hybrid pumping Application. Journal Européen des Systèmes Automatisés, 53(5): 601-608.

http://doi.org/10.18280/jesa.530502

Adjati A., Rekioua T., Rekioua D. (2021) Use of the Dual Stator Induction Machine in Photovoltaic - Wind Hybrid Pumping, Journal Européen des Systèmes Automatisés, Vol.54, N°.1, pp. 115-124.

Adjati A. (2022) Etude des machines asynchrones à double étoile en pompage hybride à énergies renouvelables. Doctoral thesis in science, University A. Mira Bejaia, Algeria,

Bajpai P., Dash V. (2012) Hybrid renewable energy systems for power generation in stand-alone applications: A review, Renew. Sustain. Energy Rev., vol. 16, no. 5, pp. 2926-2939.

doi: 10.1016/j .rser.2012 .02.009

Bemal-Agustin L, Dufo-Lapez R. (2009) Simulation and optimization of standalone hybrid renewable energy systems. Renew. Sustain. Energy Rev., vol. 13, pp. 2111 - 2118.

doi: 10.1016/j.rser.2009.01.010.

Bouzidi B. (2011) Viability of solar or wind for water pumping systems in the Algerian Sahara regions case study Adrar. Renewable and Sustainable Energy Reviews. 15:4436-42.

Cropper M. A. J., Geiger S., Jollie D. M. (2004) Fuel cells: a survey of current developments. Journal of Power Sources, vol. 131, n° 1-2, pp. 57-61.

Dufo-Lapez R., Bemal-Agustin J. L. (2009) Simulation and optimization of standalone hybrid renewable energy systems. Renew. Sustain. Energy Rev., vol. 13, pp. 2111 - 2118.

doi: 10.1016/j.rser.2009.01.010.

Hajdidj, M.S., Bibi-Triki, N., Didi, F. (2017) Study and optimization of a renewable system of small power generation. European Journal of Electrical Engineering, 19(3-4): 133-154. https://doi.org/10.3166/EJEE.19.133-154.

Hamitouche K., Chekkal S., Amimeur H., Aouzellag D. (2020) A new control strategy of dual stator induction generator with power regulation. Journal Européen des Systèmes Automatisés : 53:469-478.

Ipsakis D., Voutetakis S., Seferlis P., Stergiopoulos F., and Elmasides C. (2009) Power management strategies for a stand-alone power system using renewable energy sources and hydrogen storage. Int. 1. Hydrogen Energy, vol. 34, no. 16, pp. 7081- 7095.

Kasbadji Merzouk N., Merzouk M., Messen N. et Benyoucef B. (2003) Profil Vertical de la Vitesse du Vent en milieu semi-aride. Test des modèles d'Extrapolation. International congress on Photovoltaic and wind energy, Tlemcen.

Zarour L. (2010) Etude technique d'un système d'énergie hybride photovoltaique-eolien hors réseau. Doctorat en électrotechnique, Mentouri University Constantine.